Inorganic Chemistry
Article
pubs.acs.org/IC

Step by Step Assembly of Polynuclear Lanthanide Complexes with a Phosphonated Bipyridine Ligand

Nabila Souri,[†,‡] Pingping Tian,[†] Alexandre Lecointre,[†] Zoé Lemaire,[†] Salah Chafaa,[‡] Jean-Marc Strub,[§] Sarah Cianférani,[§] Mourad Elhabiri,[∥] Carlos Platas-Iglesias,[⊥] and Loïc J. Charbonnière*,[†]

[†]Laboratoire d'Ingénierie Moléculaire Appliquée à l'Analyse, Institut Pluridisciplinaire Hubert Curien (IPHC, UMR 7178), CNRS-Université de Strasbourg,, ECPM, 25, rue Becquerel, 67087 Strasbourg Cedex, France

[‡]Laboratoire d'électrochimie des Matériaux Moléculaires et des Complexes, LEMMC, Faculté de Technologie, Université de Sétif-1, Sétif, Algeria

[§]Laboratoire de Spectrométrie de Masse Bio-Organique, IPHC, UMR 7178, CNRS-Université de Strasbourg, ECPM, 25, rue Becquerel, 67087 Strasbourg, France

[∥]Laboratoire de Chimie Bioorganique et Médicinale, UMR 7509, CNRS-Université de Strasbourg, ECPM, 25, rue Becquerel, 67087 Strasbourg Cedex 02, France

[⊥]Universidade da Coruña, Centro de Investigacións Científicas Avanzadas (CICA) and Departamento de Química Fundamental, Facultade de Ciencias, 15071 A Coruña, Galicia, Spain

S *Supporting Information*

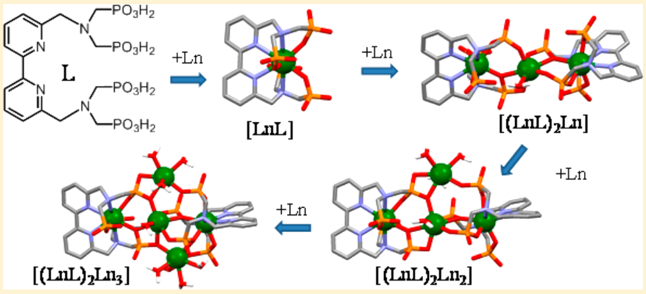

ABSTRACT: The synthesis of the octadentate ligand L (LH_8 = ((([2,2′-bipyridine]-6,6′-diylbis(methylene))bis(azanetriyl))tetrakis(methylene))tetrakis(phosphonic acid)) is reported. The coordination of L with various lanthanide cations was monitored by absorption and luminescence spectrophotometric titration experiments (Ln = Tb, Yb), potentiometry (Ln = La, Eu, Lu), and mass spectrometry (Ln = Tb). It was found that L forms very stable mononuclear (LnL) species in aqueous solutions ($\log K$ = 19.80(5), 19.5(2), and 19.56(5) for La, Eu, and Lu, respectively) with no particular trend along the series. Spectroscopic data showed the Ln cations to be enclosed in the cavity formed by the octadentate ligand, thereby shielding the metal from interactions with water molecules in the first coordination sphere. When more than one equivalent of cations is added, the formation of polynuclear $[(LnL)_2Ln_x]$ complexes (x = 1−3) can be observed, the presence of which could be confirmed by electrospray and MALDI mass spectrometry experiments. DFT modeling of the mononuclear (LnL) complexes indicated that the coordination of the cation in the cavity of the ligand results in a very asymmetric charge distribution, with a region of small negative electrostatic potential on the hemisphere composed of the chromophoric bipyridyl moiety and an electron-rich domain at the opposite hemisphere around the four phosphonate functions. DFT further showed that this polarization is most likely at the origin of the strong interactions between the (LnL) complexes and the incoming additional cations, leading to the formation of the polynuclear species. ^1H and ^{31}P NMR were used to probe the possible exchange of the lanthanide complexed in the cavity of the ligand in D_2O, revealing no detectable exchange after 4 weeks at 80 °C and neutral pD, therefore pointing out an excellent kinetic inertness.

INTRODUCTION

Phosphonated ligands have long been shown to be excellent chelators for the coordination of the hard Lewis acid cations of the lanthanide (Ln) series.[1] Their second pK_a values are close to neutrality in aqueous solutions,[2] affording strong electrostatic interactions with the trivalent Ln cations. In comparison to carboxylate analogues, phosphonates are bulkier and bring larger steric hindrance.[3] For luminescent applications,[4] this property is particularly important with respect to the necessity of shielding the luminescent Ln cations from solvent molecules, particularly those of water, at the origin of important losses in luminescence efficiency by nonradiative vibrational quenching.[5]

In polyamino-functionalized ligands, replacement of carboxylates by phosphonates generally leads to a decrease in the number of water molecules coordinated in the first sphere of Ln.[6] Although it is beneficial for the luminescence properties, this water displacement has been shown to be detrimental for the corresponding Gd complexes used as contrast agents for nuclear magnetic resonance imaging such as in the case of GdDOTP, lacking water molecules in the first coordination sphere.[7] Phosphonate functions also display a very versatile

Received: October 4, 2016

DOI: 10.1021/acs.inorgchem.6b02414

Scheme 1. Heteroaromatic Phosphonated Ligands

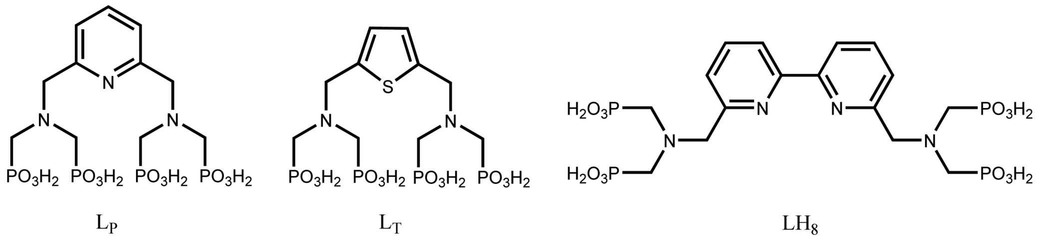

coordination chemistry, potentially acting as monodentate, bidentate, or bridging coordination units. Finally, phosphonated complexes often display important second-sphere interactions, particularly with water surroundings in aqueous media.[8]

Within the frame of our ongoing research on phosphonated chelates, we recently reported the Ln coordination properties of pyridine- and thiophene-based ligands functionalized with two aminobis(methylenephosphonate) coordinating arms, L_P[9] and L_T,[10] respectively (Scheme 1).

In the case of L_P, the presence of the phosphonate functions was shown to lead to extremely stable complexes in water, with excellent relaxation properties of the Gd(III) complex.[9a] However, luminescence studies revealed the presence of a water molecule that fulfills the first coordination sphere of the eight-coordinated Ln(III) cation in the cavity of the heptadentate ligand. We thus turned our attention toward the bipyridyl analogue L, succinctly studied by Mukkala and coworkers,[11] expecting that the introduction of an additional pyridyl ring would remove the water molecule and improve the shielding of the cation in the complexes. Herein, we report on a new synthesis of ligand L and on a detailed thermodynamic and kinetic analysis of its coordination behavior with Ln(III) cations.

■ EXPERIMENTAL SECTION

Synthesis of the Ligand and Complexes. Solvents and starting materials were purchased from Aldrich, Acros, and Alfa Aesar and used without further purification. Column chromatography and flash column chromatography were performed with silica (0.063−0.200 mm, Macherey-Nagel) or silica gel (40−63 μm, Macherey-Nagel). ^1H, ^{13}C, and ^{31}P NMR spectra were recorded at room temperature on Bruker Avance 300 and Avance 400 spectrometers operating at 300 and 400 MHz for ^1H, respectively. When unspecified, coupling constants refer to H−H coupling. Chemical shifts are reported in ppm, with residual protonated solvent as the internal reference.[12] IR spectra were recorded on a PerkinElmer Spectrum One spectrophotometer as solid samples, and only the most significant absorption bands are given in cm^{-1}. Elemental analysis were performed by the service commun d'analyse of the University of Strasbourg. High-performance ionic chromatography (HPIC) was performed at the Plateforme d'analyse inorganique of the chemistry school of Strasbourg. Diethyl 2,2′-bipyridine-6,6′-dicarboxylate[13] and tetraethyl *N*-benzyliminobis(methanephosphonate)[14] were prepared according to literature procedures.

Tetraethyl Iminobis(methanephosphonate). In a 50 mL two-necked round-bottom flask equipped with a condenser, tetraethyl *N*-benzyliminobis(methanephosphonate)[14] (2.0 g, 4.9 mmol) was dissolved in 20 mL of EtOH and 300 mg of 10% Pd/C was added. A stream of H_2 was bubbled through the solution, and the mixture was brought to reflux. After 3 h, the solution was cooled to room temperature, filtered, and evaporated to dryness. The crude residue was purified by chromatography (SiO_2, CH_2Cl_2/MeOH 100/0 to 94/6) tetraethyl iminobis(methanephosphonate) (1.48 g, 4.66 mmol, 96%) as a colorless oil. Analytical data correspond to those reported in the literature.[14]

Synthesis of 6,6′-Bis(hydroxymethyl)-2,2′-bipyridine (1). 2,2′-Bipyridine-6,6′-dicarboxylic acid diethyl ester (1.0 g, 3.33 mmol) was dissolved in methanol (15 mL). The mixture was stirred for 30 min at 0 °C, and $NaBH_4$ (0.5 g, 4 eq, 13.3 mmol) was added slowly. The solution was stirred for 3 days at 60 °C under an argon atmosphere. Water was added, and the pH was adjusted to 6 with 2 M HCl. The mixture was extracted with CH_2Cl_2 (3 × 80 mL) and dried over $NaSO_4$, and the organic solution was concentrated under vacuum to give compound **1** (0.72 g, 85%). Analytical data correspond to those reported in the literature.[15]

6,6′-Bis(bromomethyl)-2,2′-bipyridine (2). 6,6′-Bis(hydroxymethyl)-2,2′-bipyridine (0.6 g, 2.77 mmol) was dissolved in dry DMF (20 mL) and cooled to 0 °C, and PBr_3 (1.31 mL, 13.9 mmol, 5 equiv) was added dropwise with a syringe. The yellow-brown suspension was stirred at 60 °C for 24 h. The solvent was removed under reduced pressure, and H_2O (20 mL) was cautiously added with ice cooling. The pH was adjusted to 6 with saturated $NaHCO_3$, and the aqueous phase was extracted with Et_2O (3 × 100 mL). The combined organic phases were dried over Na_2SO_4, filtered, and evaporated to dryness. The yellow solid residue was purified by column chromatography (SiO_2, CH_2Cl_2 100%) to give compound **2** (0.65 g, 68%). Analytical data correspond to those reported in the literature.[16]

Synthesis of Compound 3. To a mixture of compound **2** (0.650 g, 1.9 mmol) and tetraethyl iminobis(methanephosphonate) (2.0 g, 6.33 mmol) in CH_3CN under a nitrogen atmosphere was added flame-dried K_2CO_3 (0.54 g, 0.62 mol). The mixture was refluxed for 6 days. After filtration, the solvent was evaporated under vacuum. The crude oil was partitioned between water and CH_2Cl_2, and the aqueous phase was washed with CH_2Cl_2 (2 × 100 mL). The combined organic phases were dried over Na_2SO_4, and the organic solution was concentrated under vacuum to give compound **3** (0.428 g, 28%). ^1H NMR ($CDCl_3$, 300 MHz): δ 8.25 (d, J = 7.5 Hz, 2 H), 7.73 (t, J = 7.5 Hz, 2H), 7.50 (d, J = 7.6 Hz, 2H), 4.22−3.96 (m, 20H), 3.25 (d, J = 9.9 Hz, 8H), 1.25 (t, J = 7.1 Hz, 24H) ppm. ^{13}C NMR ($CDCl_3$, 75 MHz): δ 157.88, 155.32, 137.21, 123.56, 119.51, 62.31 (t, $^3J_{PC}$ = 10 Hz), 62.01, 50.40 (d, $^2J_{PC}$ = 100 Hz), 16.41 (d, $^3J_{PC}$ = 8.0 Hz). ^{31}P NMR ($CDCl_3$, 162 MHz): δ 24.49. IR (ATR, cm^{-1}): ν 3464 (br, ν_{O-H}), 2982 (m, ν_{CH3}), 2908 (w, ν_{CH2}), 1227 (m, $\nu_{P=O}$), 1018 (s, ν_{P-O}), 956 (s, ν_{P-C}). Anal. Calcd for $C_{32}H_{58}O_{12}P_4N_4 \cdot H_2O$: C, 46.14; H, 7.26; N, 6.73. Found: C, 46.38; H, 7.01; N, 6.57. ESI$^+$/MS: m/z 837.28; calcd for $[M + Na]^+$, 837.29.

Synthesis of Ligand LH_8. Compound **3** (900 mg, 1.1 mmol) was dissolved in concentrated HCl (5 mL), and the mixture was refluxed overnight. The solvent was evaporated under reduced pressure to give ligand LH_8 as its dihydrochloride salt (0.464 g, 62%) as a pale yellow powder. ^1H NMR (D_2O, 300 MHz): δ 8.52 (d, $^3J_{HH}$ = 8.0 Hz, 2H), 8.37 (t, $^3J_{HH}$ = 7.8 Hz, 2H), 7.90 (d, $^3J_{HH}$ = 7.9 Hz, 2H), 5.03 (s, 4H), 3,58 (d, $^2J_{PH}$ = 12.3 Hz, 8H). ^{13}C NMR (D_2O, 100 MHz): δ 148.79, 147.66, 144.34, 128.40, 124.37, 58.21 (br), 52.43 (dd, $^1J_{PC}$ = 188 Hz, ^3J = 3.9 Hz). ^{31}P NMR (D_2O, 162 MHz): δ 8.35. IR (ATR, cm^{-1}): ν 2653 (br, ν_{OH}), 1166 (m, $\nu_{P=O}$), 908 (s, ν_{P-C}). Anal. Calcd for $C_{16}H_{26}N_4O_{12}P_4 \cdot H_2O \cdot 2HCl$: C, 28.21; H, 4.43; N, 8.22. Found: C, 28.49; H, 4.44; N, 8.36. HPIC: Cl, 11.4(8)%; calcd for $LH_8 \cdot H_2O \cdot 2HCl$, 10.4%. ESI$^+$/MS: m/z 591.06; calcd for $[M + H]^+$, 591.06.

Synthesis of the Ln(III) Complexes. *[LaL].* Ligand L (30.3 mg, 44 μmol) and $LaCl_3{\cdot}7H_2O$ (16.1 mg, 43 μmol) were dissolved in water (4 mL). A dilute NaOH solution was added to raise the pH to 7, and the mixture was stirred at room temperature overnight. Addition of EtOH resulted in the precipitation of the complex, which was isolated by centrifugation and dried under reduced pressure to give [LaL] (25 mg, 64%) as a white powder. ^{1}H NMR (D_2O, pD 7.4, 400 MHz): δ 8.24 (d, J = 8.1 Hz, 2H), 8.11 (t, J = 6.4 Hz, 2H), 7.59 (d, J = 7.4 Hz, 2H), 5.06 (s, br, 4H) ppm. ^{13}C NMR (D_2O, 100 MHz): δ 158.54, 154.88, 140.58, 125.44, 121.44, 61.28 (t, $^3J_{PC}$ = 8 Hz), 56.13 ppm (dd, $^1J_{PC}$ = 142 Hz, $^3J_{PC}$ = 8 Hz). ^{31}P NMR (D_2O, 162 MHz): δ 20.26 ppm. IR (ATR, cm^{-1}): ν 3206 (br, ν_{O-H}), 1264 (w, $\nu_{P=O}$), 1050 (s, ν_{P-O}), 973 (s). ESI$^-$/MS: m/z 724.91; calcd for $C_{16}H_{22}N_4P_4O_{12}La$ ($LaLH_4^-$), 724.92.

[TbL]. Ligand L (28.3 mg, 42 μmol) and $TbCl_3{\cdot}6H_2O$ (15.1 mg, 40 μmol) were dissolved in water (3 mL). A dilute NaOH solution was added to raise the pH to 7, and the mixture was stirred at room temperature overnight. Addition of EtOH resulted in the precipitation of the complex, which was isolated by centrifugation and dried under reduced pressure to give [TbL] (35 mg, 87%) as a white powder. ESI$^-$/MS: m/z 744.95; calcd for $C_{16}H_{22}N_4P_4O_{12}Tb$ ($TbLH_4^-$), 744.94. IR (ATR, cm^{-1}): ν 3200 (br, ν_{O-H}), 1249 (w, $\nu_{P=O}$), 1048 (s, ν_{P-O}), 973 (s). Anal. Calcd for $C_{16}H_{19}N_4Na_4O_{12}P_4Tb{\cdot}7H_2O$: C, 20.01; H, 3.46; N, 5.83. Found: C, 19.68; H, 3.04; N, 5.45.

[YbL]. Ligand L (20 mg, 29.4 μmol) and $YbCl_3{\cdot}6H_2O$ (11 mg, 28.4 μmol) were dissolved in water (3.5 mL). A dilute NaOH solution was added to raise the pH to 7. The mixture was stirred at room temperature overnight. Addition of EtOH resulted in the precipitation of the complex, which was isolated by centrifugation and dried under reduced pressure to give [YbL] (20 mg, 69%) as a white powder. ^{1}H NMR (300 MHz, pD 12.4, D_2O): δ 46.81 (s, br, 2H), 39.92 (s, br, 2H), 37.25 (s, br, 2H), 32.25 (s, br, 2H), 31.14 (s, br, 2H), 24.25 (s, br, 2H), 22.50 (s, br, 2H), 13.34 (s, br, 2H), 11.67 (s, br, 2H) ppm. IR (ATR. cm^{-1}): ν 3263 (br, ν_{O-H}), 1249 (w, $\nu_{P=O}$), 1054 (s, ν_{P-O}), 984 (s). ESI$^-$/MS: m/z 759.95; calcd for $C_{16}H_{22}N_4P_4O_{12}Yb$ ($YbLH_4^-$), 759.96. Anal. Calcd for $C_{16}H_{19}N_4O_{12}P_4YbNa_4{\cdot}8H_2O$: C, 19.36; H, 3.56; N, 5.65. Found: C, 19.29; H, 3.24; N, 5.42.

[LuL]. Ligand L_H (29.2 mg, 46 μmol) and $LuCl_3{\cdot}6H_2O$ (16.3 mg, 42 μmol) were dissolved in water (4 mL). A dilute NaOH solution was added to raise the pH to 7, and the mixture was stirred at room temperature overnight. Addition of EtOH resulted in the precipitation of the complex, which was isolated by centrifugation and dried under reduced pressure to give LuL (35 mg, 81%) as a white powder. ^{1}H NMR (300 MHz, pD 7.4, D_2O): δ 8.02 (d, J = 8 Hz, 2H), 7.89 (t, J = 8 Hz, 2H), 7.30 (d, J = 8 Hz, 2H), 4.18 (s, br, 2H), 3.40−3.00 (m, br, 6H), 2.73 (s, br, 2H) ppm. ^{13}C NMR (D_2O, 100 MHz): δ 160.33, 152.48, 139.72, 122.98, 119.71, 66.02 ppm. ^{31}P NMR (D_2O, 162 MHz): δ 21.09, 18.67 ppm. ESI$^-$/MS: m/z 760.97; calcd for $C_{16}H_{22}LuN_4O_{12}P_4^-$ ($LuLH_4^-$), 760.96. IR (ATR, cm^{-1}): ν 3204 (br, ν_{O-H}), 1224 (w, $\nu_{P=O}$), 1050 (s, ν_{P-O}), 980 (s). Anal. Calcd for $C_{16}H_{19}N_4Na_4LuO_{12}P_4{\cdot}5H_2O$: C, 20.44; H, 3.11; N, 5.96. Found: C, 20.62; H, 3.26; N, 5.59.

DFT Calculations. All calculations were performed employing DFT within the hybrid meta-GGA approximation with the TPSSh exchange-correlation functional[17] and the Gaussian 09 package (Revision D.01).[18] Full geometry optimizations of $[YbL]^{5-}$, $[(YbL)_2Yb]^{7-}{\cdot}H_2O$, $[(YbL)_2Yb_2]^{4-}{\cdot}4H_2O$, and $[(YbL)_2Yb_3]^{-}{\cdot}9H_2O$ were performed in aqueous solution by using the large-core relativistic effective core potential (LCRECP) of Dolg et al. and the related (7s6p5d)/[5s4p3d]-GTO valence basis set for the lanthanides[19] and the standard 6-31G(d) basis set for C, H, N, O, and P atoms. No symmetry constraints have been imposed during the optimizations. The default values for the integration grid (75 radial shells and 302 angular points) and the SCF energy convergence criteria (10^{-8}) were used in all calculations. Bulk solvent effects (water) were considered by using the integral equation formalism variant of the polarizable continuum model (IEFPCM).[20] The universal force field radii (UFF)[21] scaled by a factor of 1.1 were used to construct the solute cavities.

Physicochemical Measurements. The starting lanthanide perchlorates ($La(ClO_4)_3$ 40 wt % solution in water, Sigma-Aldrich, 99.9%, $Tb(ClO_4)_3$ 50 wt % solution in water, Alfa Aesar, and $Lu(ClO_4)_3$, 50 wt % solution in water, Strem Chemicals, 99.9%;) are commercial products, which were used without further purification. Distilled water was further purified by passing it through a mixed bed of ion exchanger (Bioblock Scientific R3-83002, M3-83006) and activated carbon (Bioblock Scientific ORC-83005) and was deoxygenated with CO_2- and O_2-free argon (Sigma Oxiclear cartridge) before use. All stock solutions were prepared by weighing solid products using an AG 245 Mettler Toledo analytical balance (precision 0.01 mg). The ionic strength was maintained at 0.1 M with sodium perchlorate ($NaClO_4{\cdot}H_2O$, Merck, p.a.), and all measurements were carried out at 25.0(2) °C. The metal stock solutions (~3 × 10^{-2} M) were freshly prepared by dilution of appropriate volumes of the corresponding perchlorate salt aqueous stock solutions in water. The metal contents of the solutions were determined with disodium EDTA (10^{-2} M, Merck, Titriplex^{III}) according to the classical colorimetric titration (xylenol orange as indicator).[22]

Caution! Perchlorate salts combined with organic ligands are potentially explosive and should be handled in small quantities and with adequate precautions.[23]

Potentiometric Titrations. The potentiometric titrations of the free ligand L and its lanthanide metal complexes (La(III), Eu(III), and Lu(III)) were performed using an automatic titrator system 794 Basic Titrino (Metrohm) with a combined glass electrode (Metrohm 6.0234.500, Long Life) filled with 0.1 M NaCl in water and connected to a microcomputer (Tiamo light 1.2 program for the acquisition of the potentiometric data). The combined glass electrode was calibrated as a hydrogen concentration probe by titrating known amounts of perchloric acid (9.92 × 10^{-2} M from $HClO_4$, Prolabo, normapur, 70% min) with a CO_2-free sodium hydroxide solution (9.72 × 10^{-2} M from NaOH, BdH, AnalaR). The $HClO_4$ and NaOH solutions were freshly prepared just before use and titrated with sodium tetraborate decahydrate ($B_4Na_2O_7{\cdot}10H_2O$, Fluka, puriss, p.a.) and potassium hydrogen phthalate ($C_8H_5KO_3$, Fluka, puriss, p.a.), respectively, using methyl orange (RAL) and phenolphthalein (Prolabo, purum) as the indicators. Typically, 4 mL of the ligand L solution (~10^{-3} M) in the absence or in the presence of an appropriate volume of the stock Ln(III) solutions to ensure reaching $[Ln(III)]_0/[L]_0 \approx 1$ was added in a jacketed cell (Metrohm 6.0234.500) maintained at 25.0(2) °C by the flow of a Lauda E200 thermostat. An aliquot of a concentrated solution of $HClO_4$ was added to decrease the starting pH to about 2.5. A stream of argon, presaturated with water vapor, was passed over the surface of the solution. The Glee program[24] was applied to calibrate the glass electrode (standard electrode potential E_0/mV and slope of the electrode/mV pH^{-1}) and to check carbonate levels of the NaOH solutions used (<5%). The potentiometric data of L and its Ln(III) complexes (about 300 points collected over the pH range 2.5−11.5, Figure S42 in the Supporting Information) were refined with the Hyperquad 2000[25] program, which uses nonlinear least-squares methods.[26] Potentiometric data points were weighted by a formula allowing greater pH errors in the region of an end point than elsewhere. The weighting factor W_i is defined as the reciprocal of the estimated variance of measurements: $W_i = 1/\sigma_i^2 = 1/[\sigma_E^2 + (\delta E/\delta V)^2\sigma_V^2]$ where σ_E^2 and σ_V^2 are the estimated variances of the potential and volume readings, respectively. The constants were refined by minimizing the error-square sum, U, of the potentials: $U = \sum_i^N W_i(E_{obs,i} - E_{cal,i})^2$. At least three titrations were treated as single sets or as separated entities, for each system, without significant variation in the values of the determined constants. The quality of fit was judged by the values of the sample standard deviation, S, and the goodness of fit, χ^2 (Pearson's test). At σ_E = 0.1 mV (0.023 σ_{pH}) and σ_V = 0.005 mL, the values of S in different sets of titrations were between 0.4 and 0.5, and χ^2 was below 30. The scatter of residuals versus pH was reasonably random, without any significant systematic trends, thus indicating a good fit of the experimental data. The successive protonation and stability constants were calculated from the cumulative constants determined with the program. The uncertainties in the log K values

Scheme 2. Synthetic Protocol for the Preparation of Ligand L

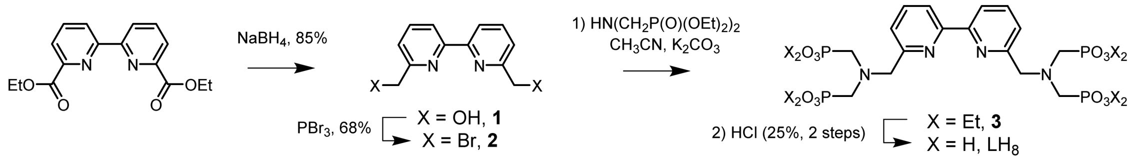

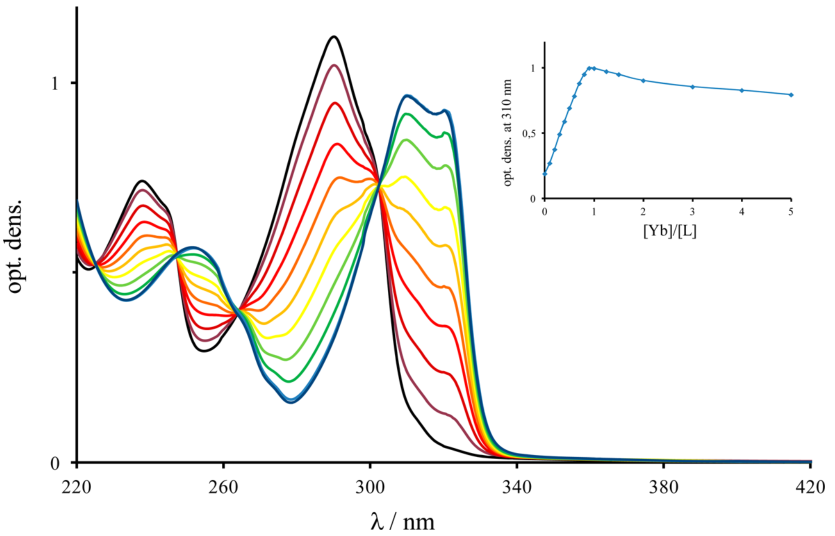

Figure 1. Evolution of the UV−vis absorption spectra of a solution of L (6.95×10^{-5} M) upon gradual addition of 1 equiv of a solution of $YbCl_3 \cdot 6H_2O$ (1.04×10^{-4} M) in TRIS/HCl (0.01 M, pH 7.4). Inset: evolution of the absorption at 310 nm as a function of the Yb(III)/L ratio for [Yb]/[L] ratio from 0 to 5.

(corresponding to 3σ with σ = standard deviation) correspond to the added standard deviations in the cumulative constants.

UV−Vis Absorption versus pH Titrations. In addition to the potentiometric investigations, absorption spectrophotometric titrations of L as a function of pH were performed. Stock solutions of L ((4−6) × 10^{-5} M) were prepared by quantitative dissolution of the corresponding solid samples in deionized water, and the ionic strength was adjusted to 0.1 M with $NaClO_4$ (Fluka, puriss). 40 mL of the solution was introduced into a jacketed cell (Metrohm) maintained at 25.0(2) °C (Lauda E200). The free hydrogen ion concentration was measured with a combined glass electrode (Metrohm 6.0234.500, Long Life) and an automatic titrator system 794 Basic Titrino (Metrohm). The Ag/AgCl reference glass electrode was filled with NaCl (0.1 M, Fluka, p.a.) and calibrated as a hydrogen concentration probe as described above. The initial pH was adjusted to ∼2−3 with $HClO_4$ (Prolabo, normapur, 70% min), and the absorption spectrophotometric titrations of L versus pH ($2.3 \lesssim$ pH $\lesssim 11$) were carried out by addition of known volumes of NaOH solutions using the automatic titrator of the 794 Basic Titrino device (DET method). After each addition, an absorption spectrum was automatically and repeatedly recorded using a Varian CARY 50 spectrophotometer fitted with Hellma optical fibers (Hellma, 041.002-UV) and an immersion probe made of quartz suprazil (Hellma, 661.500-QX) and interfaced (Cetrib) with the potentiometric unit.

UV−Vis Absorption Spectrophotometric Titrations of L by Ln(III) at pH 2. A stock solution of L (∼10^{-3} M) prepared in water was freshly diluted with $HClO_4$ (∼10^{-1} M) and $NaClO_4$ ($NaClO_4 \cdot H_2O$, Merck, p.a.) to obtain a ligand concentration of ∼9.4×10^{-5} M. The ionic strength was kept constant at 0.1 M with $NaClO_4$ and $HClO_4$. The absorption spectrophotometric titrations of L by Ln(III) (La(III), Eu(III), and Lu(III)) were then carried out on solutions at pH ∼2 (10^{-2} M $HClO_4$). Microvolumes of a concentrated solution of Ln(III) (∼3×10^{-2} M) were added to 1 mL of the ligand solution in a 1 cm path length optical cell. Special care was taken to ensure that complete equilibration was attained. The corresponding UV−vis absorption spectra were recorded from 230 to 800 nm on an Agilent Cary 5000 spectrophotometer maintained at 25.0(2) °C by the flow of a Cary Varian Dual Cell Peltier accessory.

Fluorimetric Titrations of L by Ln(III) at pH 2. The fluorimetric titrations were carried out on solutions of L with an absorbance smaller than 0.1 at wavelengths $\geq\lambda_{exc}$ (∼10^{-5} M) in order to avoid any errors due to the inner filter effects. The titrations of 3 mL of the ligand L were carried out in a 1 cm Hellma quartz optical cell by addition of known microvolumes of solution of Ln(III) (La(III), Eu(III), and Lu(III)). The excitation wavelength at 305 nm corresponded to an isosbestic point between the free ligand and the Ln(III) complexes evaluated previously. The fluorescence emission spectra were recorded from 305 to 800 nm on a PerkinElmer LS-50B instrument maintained at 25.0(2) °C by the flow of a Haake FJ thermostat. The light source was a pulsed xenon flash lamp with a pulse width at half peak height of <10 μs and power equivalent to 20 kW. The slit widths were set at 6.5 and 8 nm for both the excitation and the emission for Lu(III) and La(III), respectively, and at 15 and 20 nm for the excitation and the emission, respectively, for Eu(III).

Combined Spectrofluorimetric and UV−Vis Absorption Titrations of the Ligand by Tb(III) and Yb(III) at pH 7.4. Titrations were performed with 2 mL of 6.95×10^{-5} M solutions of L in 0.01 M TRIS/HCl buffer at pH 7.4 to which were added increasing amounts of $TbCl_3 \cdot 6H_2O$ at 1.24×10^{-3} M (or $YbCl_3 \cdot 6H_2O$ at 1.04×10^{-3} M) in the same buffer. After each addition, the UV−vis absorption spectra were recorded from 210 to 400 nm and the emission spectra were recorded from 450 to 700 nm for Tb(III) and from 850 to 1150 nm for Yb(III) upon excitation at 290 nm. In the case of Yb(III), a high-pass filter at 850 nm was used to remove second-order excitation artifacts.

Analysis and Processing of the Spectroscopic Data. The spectrophotometric data were analyzed with the Specfit[27−29] program, which adjusts the absorptivities and the stability constants of the species formed at equilibrium. Specfit uses factor analysis to reduce the absorbance matrix and to extract the eigenvalues prior to the multiwavelength fit of the reduced data set according to the Marquardt algorithm.[30,31]

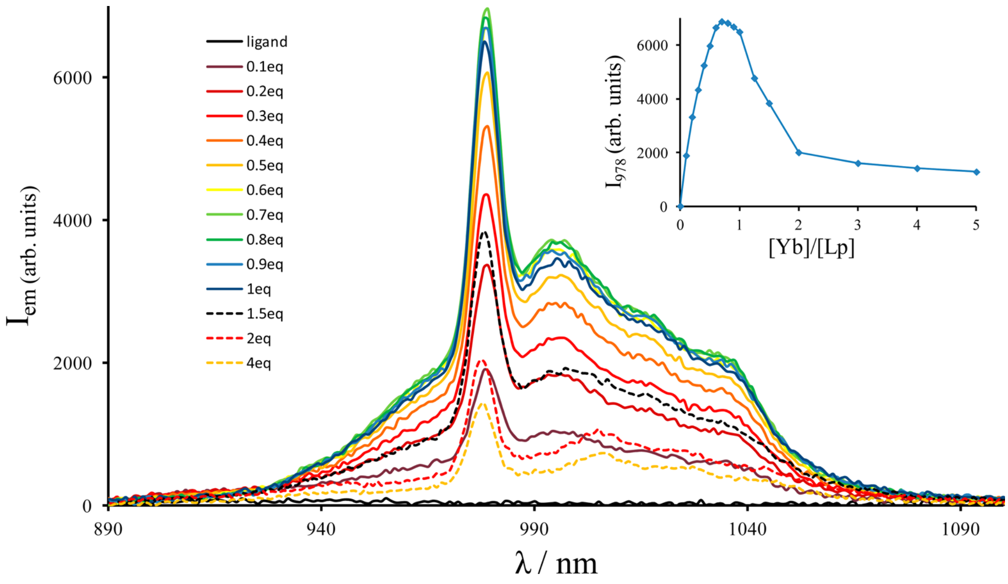

Figure 2. Evolution of the NIR luminescence spectra of a solution of L (6.95×10^{-5} M) upon addition of aliquots of $YbCl_3 \cdot 6H_2O$ (1.04×10^{-4} M) in TRIS/HCl (0.01 M, pH 7.4, λ_{exc} 290 nm). Inset: evolution of the emitted luminescence intensity at 978 nm as a function of the Yb/L ratio.

Table 1. Successive Protonation Constants of Ligand L[a]

Equilibria	log K_{LHx}	
$L^{8-} + H^+ \overset{K_{LH}}{\rightleftharpoons} LH^{7-}$	10.89(2)[b]	$$KLH_x = \frac{[LH_x]}{[LH_{x-1}][H^+]}$$
$LH^{7-} + H^+ \overset{K_{LH2}}{\rightleftharpoons} LH_2^{6-}$	10.27(2)[b]	
$LH_2^{6-} + H^+ \overset{K_{LH3}}{\rightleftharpoons} LH_3^{5-}$	6.95(4)[b]	
$LH_3^{5-} + H^+ \overset{K_{LH4}}{\rightleftharpoons} LH_4^{4-}$	6.21(5)[b]	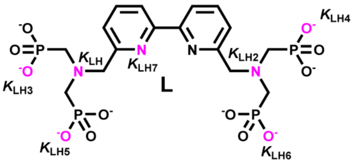
$LH_4^{4-} + H^+ \overset{K_{LH5}}{\rightleftharpoons} LH_5^{3-}$	5.49(6)[b]	
$LH_5^{3-} + H^+ \overset{K_{LH6}}{\rightleftharpoons} LH_6^{2-}$	4.63(7)[b]	
$LH_6^{2-} + H^+ \overset{K_{LH7}}{\rightleftharpoons} LH_7^{-}$	2.45(9)[b] / 2.1(2)[c]	

[a] Conditions: solvent, water; $I = 0.1$ M $NaClO_4$; $T = 25.0(2)$ °C, error 3σ with σ = standard deviation. [b] Obtained from potentiometric titrations. [c] Obtained from absorption spectrophotometric titrations vs pH. From the UV−vis absorption versus pH titrations, two pK_a values were determined at 10.72(9) and 5.44(5) and likely correspond to the average protonation constants of the two tertiary amines and the four phosphonate units, respectively.

Mass Spectrometry. ES/MS experiments were performed on a hybrid electrospray quadrupole time-of-flight (TOF) mass spectrometer MS (Synapt G2 HDMS, Waters, Manchester, U.K.) coupled to an automated chip-based nanoelectrospray device (Triversa Nanomate, Advion Biosciences, Ithaca, NY, USA) operating in the positive ion mode. The MS analysis was performed on the Synapt G2 HDMS instrument with external calibration using the singly charged ions produced by an ES-TOF tuning mix (G1969-85000, Agilent, USA) and classical interface tuning parameters of the mass spectrometer (V_c = 40 V, P_i = 2.1 mbar).

MALDI/TOF mass measurements were carried out on an Autoflex MALDI-TOF mass spectrometer (Bruker Daltonics GmbH, Bremen, Germany). This instrument was used at a maximum accelerating potential of 20 kV in the positive mode and was operated in mode reflector at 19 kV. The delay extraction was fixed at 60 ns, and the frequency of the laser (nitrogen 337 nm) was set at 5 Hz. The acquisition mass range was set to m/z 400−4000 with a matrix suppression deflection (cut off) set to m/z 500. The equipment was externally calibrated with a standard peptide calibration mixture that contained seven peptides (Bruker Peptide Calibration Standard #206196, Bruker Daltonics GmbH, Bremen, Germany) covering the *m*/*z* 1000−3200 range. Each raw spectrum was opened with flexAnalysis 2.4 build 11 (Bruker Daltonics GmbH, Bremen, Germany) software and processed using the following parameters: signal to noise threshold of 1, Savitzky−Golay algorithm for smoothing, median algorithm for baseline subtraction, and SNAP algorithm for monoisotopic peak detection and labeling. Sample preparation was performed with the dried droplet method using a mixture of 0.5 μL of sample with 0.5 μL of matrix solution dried at room temperature. The matrix solution was prepared from a saturated solution of α-cyano-4-hydroxycinnamic acid in water/acetonitrile 50/50 diluted three times in water/acetonitrile/trifluoroacetic acid 50/49.9/0.1.

RESULTS AND DISCUSSION

The synthesis of ligand L is presented in Scheme 2, and full experimental details can be found in the Experimental Section.

Table 2. Stability Constants (log K_{LnL}) for the Formation of the LnL Complexes in H_2O (Ln(III) = La(III), Eu(III), Lu(III), 0.1 M $NaClO_4$, 25.0(2) °C) and the Associated Protonation Constants[a]

	M = La(III)	M = Eu(III)	M = Lu(III)
$K_{\mathrm{ML}} = \frac{[\mathrm{ML}]}{[\mathrm{M}][\mathrm{L}]}$			
log K_{ML}	19.80(5)	19.5(2)	19.56(5)
$K_{\mathrm{MLHx}} = \frac{[\mathrm{MLH}_x]}{[\mathrm{MLH}_{x-1}][\mathrm{H}^+]}$			
log K_{MLH}	7.41(6)	8.3(2)	8.77(6)
log K_{MLH2}	6.41(7)	6.4(2)	6.77(7)
log K_{MLH3}	5.42(7)	5.4(2)	5.47(7)
log K_{MLH4}	3.95(7)	3.5(3)	3.33(7)
log $K_{\mathrm{M(OH)L}}$	−10.97(8)	−10.51(2)	−10.42(8)
log $K_{\mathrm{M(OH)}}$	−8.83	−7.78	−7.29
pLn(L)[b]	14.56	14.78	15.12
pLn(L)[c]	9.80	9.91	10.08
pLn(L_P)[b]	21.24	21.40	23.1
pLn(L_P)[c]	13.13	13.36	14.24

[a] Error =3σ with σ = standard deviation. Charges are omitted for the sake of clarity. [b] pLn = [Ln(III)] calculated for [L] = 10^{-5} M, [Ln] = 10^{-6} M, pH 7.4. [c] pLn = [Ln(III)] calculated for [L] = 10^{-6} M, [Ln] = 10^{-6} M, pH 7.4.

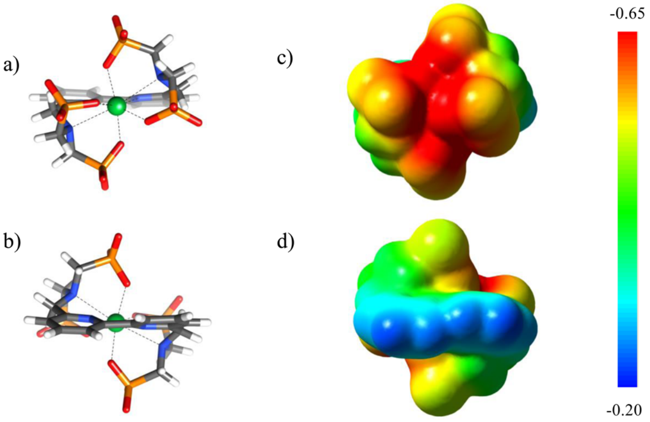

Figure 3. DFT models of the $[\mathrm{YbL}]^{5-}$ complex in aqueous solution viewed perpendicularly to its pseudo-C_2 axis with phosphonate functions pointing toward the front (a) or the back (b) of the page and (c, d) the corresponding computed TPSSh/LCRECP/6-31G* electrostatic potential (in hartrees) on the molecular surface defined by 0.001 electron bohr^{-3} contour of the electronic density.

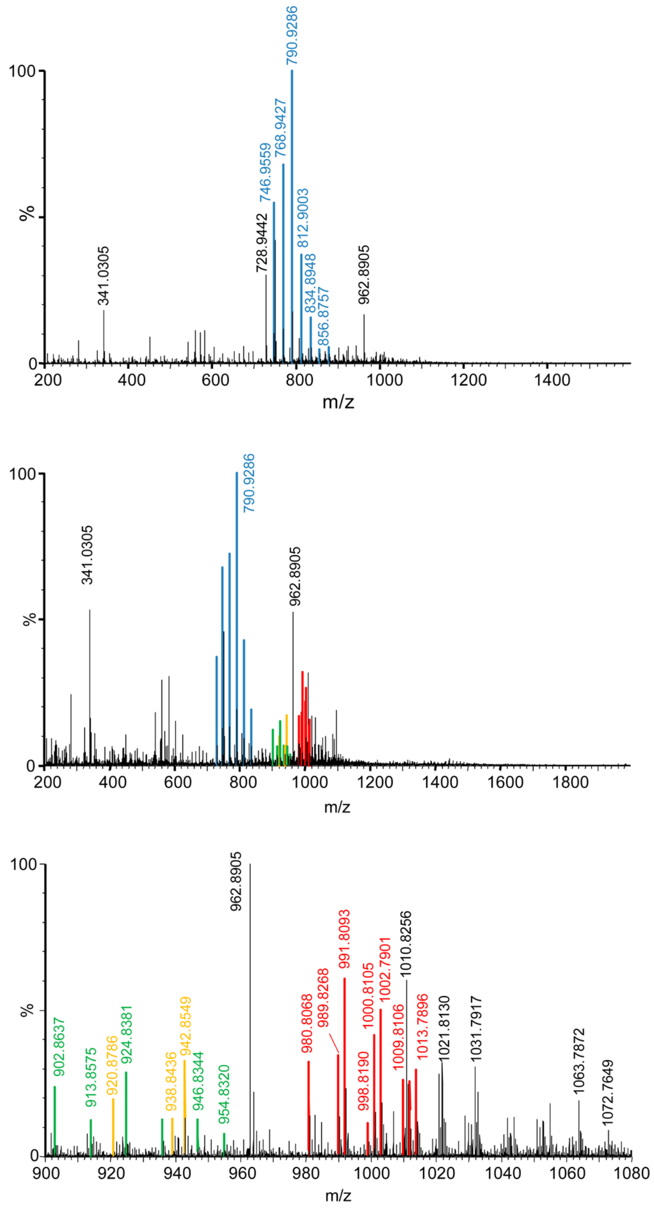

Figure 4. ESI-MS spectra of a solution of [TbL] in water (pH 2) without (top) and with 1 equiv (middle and bottom) of $TbCl_3 \cdot 6H_2O$. Color code: species attributed to [TbL] (blue), $[Tb_2L]$ (orange), $[Tb_4L_2]$ (green), and $[Tb_5L_2]$ (red) stoichiometries.

The ligand was isolated in an overall yield of 14% over the four steps. This represents a significant improvement with respect to the procedure of Mukkala et al.,[11] which required three steps with a low overall yield of ∼3% to give the 2,2′-bipyridine-6,6′-bis(methylamine) precursor, followed by a Mannich reaction with formaldehyde and phosphorous acid yielding L, which was directly used for metal ion complexation.[11]

The coordination of lanthanide cations (Ln(III) = Tb(III), Yb(III)) with L was first investigated using a combination of UV−vis absorption spectroscopy and steady-state and time-resolved luminescence spectroscopy. Titration experiments were carried out by adding increasing amounts of the trivalent cations to a 0.01 M TRIS/HCl aqueous solution of the ligand at pH 7.4. Figure 1 displays the evolution observed during the titration of L by Yb(III) as observed by absorption spectrophotometry. The corresponding evolution for the

Table 3. Attribution of the Peaks Observed in the ES/MS Spectra of a Solution of TbL Titrated by Addition of Tb(III)

species	formulation	chem formula	calcd monoisotopic mass[a]	measd mass
TbL	$[TbLH_6]^+$	$C_{16}H_{24}N_4P_4O_{12}Tb$	746.9595	746.9559
	$[TbLH_5Na]^+$	$C_{16}H_{23}NaN_4P_4O_{12}Tb$	768.9414	768.9427
	$[TbLH_4Na_2]^+$	$C_{16}H_{22}Na_2N_4P_4O_{12}Tb$	790.9233	790.9286
	$[TbLH_3Na_3]^+$	$C_{16}H_{21}Na_3N_4P_4O_{12}Tb$	812.9053	812.9128
	$[TbLH_2Na_4]^+$	$C_{16}H_{20}Na_4N_4P_4O_{12}Tb$	834.8872	834.8948
	$[TbLHNa_5]^+$	$C_{16}H_{19}Na_5N_4P_4O_{12}Tb$	856.8691	856.8757
	$[TbLNa_6]^+$	$C_{16}H_{18}Na_6N_4P_4O_{12}Tb$	878.8511	878.8570
Tb_4L_2	$[Tb_4L_2H_6]^{2+}$	$C_{32}H_{42}N_8O_{24}P_8Tb_4$	902.8608	902.8637
	$[Tb_4L_2H_5Na]^{2+}$	$C_{32}H_{41}NaN_8O_{24}P_8Tb_4$	913.8518	913.8575
	$[Tb_4L_2H_4Na_2]^{2+}$	$C_{32}H_{40}Na_2N_8O_{24}P_8Tb_4$	924.8427	924.8381
	$[Tb_4L_2H_3Na_3]^{2+}$	$C_{32}H_{39}Na_3N_8O_{24}P_8Tb_4$	935.8337	935.8307
	$[Tb_4L_2H_2Na_4]^{2+}$	$C_{32}H_{38}Na_4N_8O_{24}P_8Tb_4$	946.8249	946.8344
Tb_2L	$[Tb_2LH_3 \cdot H_2O]^+$	$C_{16}H_{23}N_4O_{13}P_4Tb_2$	920.8713	920.8786
	$[Tb_2LH_3 \cdot 2H_2O]^+$	$C_{16}H_{25}N_4O_{14}P_4Tb_2$	938.8819	938.8436
	$[Tb_2LH_2Na \cdot H_2O]^+$	$C_{16}H_{22}NaN_4O_{13}P_4Tb_2$	942.8533	942.8549
Tb_5L_2	$[Tb_5L_2H_3]^{2+}$	$C_{32}H_{39}N_8O_{24}P_8Tb_5$	980.8068	980.8117
	$[Tb_5L_2H_3 \cdot H_2O]^{2+}$	$C_{32}H_{41}N_9O_{25}P_8Tb_5$	989.8268	989.8170
	$[Tb_5L_2H_2Na]^{2+}$	$C_{32}H_{38}NaN_8O_{24}P_8Tb_5$	991.8093	991.8027
	$[Tb_5L_2H_3 \cdot 2H_2O]^{2+}$	$C_{32}H_{43}N_9O_{26}P_8Tb_5$	998.8190	998.8223
	$[Tb_5L_2H_2Na \cdot H_2O]^{2+}$	$C_{32}H_{40}NaN_8O_{25}P_8Tb_5$	1000.8105	1000.8079
	$[Tb_5L_2HNa_2]^{2+}$	$C_{32}H_{37}Na_2N_8O_{24}P_8Tb_5$	1002.7901	1002.7937
	$[Tb_5L_2H_2Na \cdot 2H_2O]^{2+}$	$C_{32}H_{42}NaN_8O_{26}P_8Tb_5$	1009.8106	1009.8137
	$[Tb_5L_2Na_3]^{2+}$	$C_{32}H_{36}Na_3N_8O_{24}P_8Tb_5$	1013.7896	1013.7846
	$[Tb_5L_2HNa_2 \cdot H_2O]^{2+}$	$C_{32}H_{39}Na_2N_8O_{25}P_8Tb_5$	1011.7989	1011.7989

[a] Considering the global charge of the species and calculated with Chemcalc.[45]

titration with Tb(III) is very similar and can be found in Figure S1 in the Supporting Information. Between 0 and 1 equiv of the added Ln(III), the evolution is monotonous, displaying a bathochromic shift of the maximum of the $\pi \rightarrow \pi^*$ absorption band of the bipyridyl moiety from 289 nm (free ligand) to 310 nm (1 equiv of Ln(III)). The presence of an isosbestic point at 301 nm is strongly indicative of the formation of a single new species. This behavior is typical of the coordination of cations to the N,N-bidentate site of the bipyridine moiety and is related to the trans to cis isomerization of the heteroaromatic core,[32,33] indicating that the first Ln(III) cation is positioned inside the coordination cavity of the ligand. Above 1 equiv, the spectral variations are less significant but nevertheless point to the formation of other species. This observation is clearly confirmed by the followup of the titration by luminescence spectroscopy (Figure 2). Upon excitation into the ligand absorption band at 290 nm, the addition of Yb(III) to the ligand solution led to the observation of an intense NIR emission centered at 978 nm, which was attributed to the characteristic $^2F_{5/2} \rightarrow {}^2F_{7/2}$ emission of Yb.[34] This behavior is typical of the antenna effect generated by the photoinduced ligand to Yb energy transfer.[35] The Yb(III)-centered luminescence intensity gradually increased up to 1 equiv and then strongly decreased up to ca. 2.5 equiv.

The marked inflection point observed at 1 equiv reflects a high stability constant for the mononuclear LnL species. After more than 1 equiv, only minor changes could be observed on the absorption spectra, while the emission spectra keep on evolving, evidencing the presence of polynuclear species, which were also observed in the emission spectra recorded during the titration with Tb(III) (Figure S5 in the Supporting Information). A global analysis of the different titration experiments was performed with the Specfit program.[26−28] Full details of the analysis (best models, calculated spectra, evolution of the concentrations of the species formed) can be found in Figures S1−S14 and Tables S1−S4 in the Supporting Information. The mathematical treatment of the data revealed two important points. The first is the formation of species with M:L stoichiometric ratios of 1:1, 3:2, 4:2, and 5:2. Depending on the amplitude of the observed variations, all of the species are not observed simultaneously. For example, the weak variations monitored by absorption spectroscopy after addition of more than 1 equiv of Ln(III) did not allow for the observations of all the species with M:L ratios higher than 1. The second important point is that the marked inflection point observed at 1 equiv is characteristic of a very stable 1:1 complex. In these conditions, the stability constants determined by this fitting procedure have to be taken with great care, and if the fitting results are excellent qualitative information (shape of the spectra, evolution of the species formed), quantitative thermodynamic data must be handled with great care.

To get further insights into the evaluation of the stability constant of the 1:1 complex formed in aqueous solution, we turned our attention to potentiometric measurements. In a first step, the pK_a values of the ligand were determined by potentiometric titrations of L in water (0.1 M $NaClO_4$) following the pH of the solution upon basification of the medium. The potentiometric titration curves are presented in Figure S15 in the Supporting Information, and the pK_a values derived from these titrations are presented in Table 1, together with the proposed attribution of the protonation sites on the associated figure. The corresponding distribution diagrams of the different protonated species can be found in Figure S16 in the Supporting Information. In parallel, UV−vis absorption spectrophotometric titrations of L as a function of pH were also recorded and provided complementary information on the acid−base properties of ligand L. The pK_a values obtained by absorption spectroscopy are gathered in Table 1, while the

DOI: 10.1021/acs.inorgchem.6b02414
Inorg. Chem. XXXX, XXX, XXX−XXX

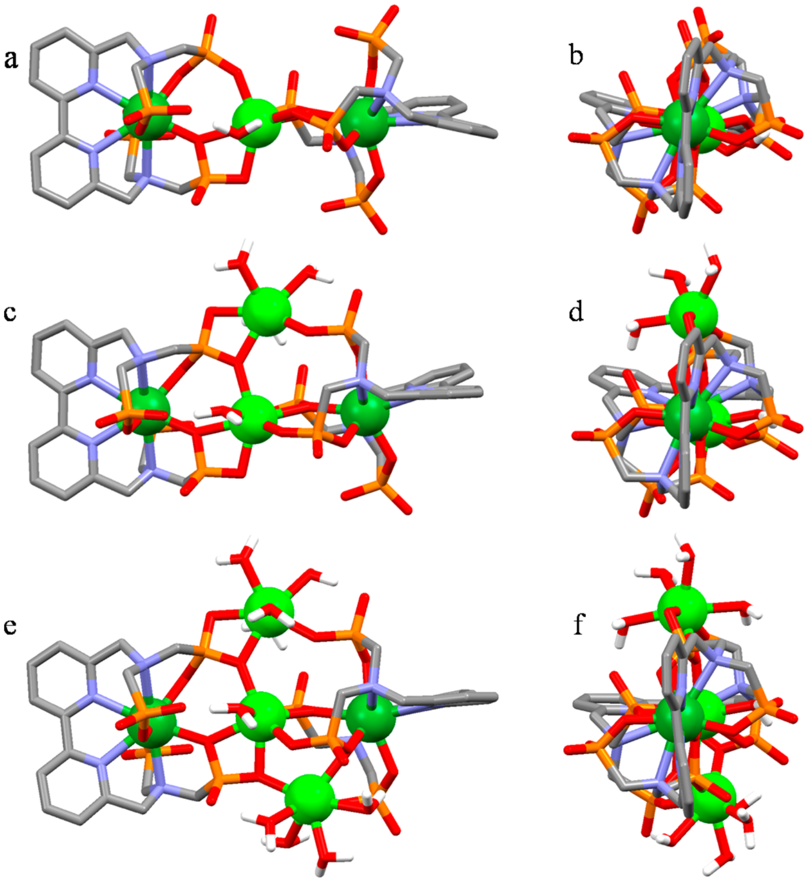

Figure 5. DFT models of the trinuclear ($[(YbL)_2Yb]$; a, b), tetranuclear ($[(YbL)_2Yb_2]$; c, d), and pentanuclear ($[(YbL)_2Yb_3]$; e, f) complexes viewed along (a, c, e) and perpendicular to (b, d, f) the Yb1−Yb2 axis. Yb(III) cations coordinated inside the cavity of the ligands appear in dark green, the additional Yb(III) cations being colored in light green. Additional color scheme: C, gray; N, blue; P, orange; O, red. H atoms are omitted for the sake of clarity except for water molecules.

spectra recorded as a function of pH and the calculated electronic spectra obtained from the fitting procedure are presented in Figures S17 and S18 in the Supporting Information.

In agreement with comparable pK_a values obtained on L_P,[9] L_T,[10] and other related polyaminophosphonated ligands,[36] the two highest protonation constants can safely be attributed to the protonation of the tertiary amines. In comparison to the analogous aminocarboxylate ligands, the pK_a values of these amines are strongly influenced by the negative charge of the adjacent phosphonate functions. The four following pK_a values were assigned to the first protonation of the four phosphonate functions. The average basicity of L (pK_a^{av} = 5.82) is comparable to those measured for L_P (pK_a^{av} = 6.06)[9] or L_T (pK_a^{av} = 5.65).[10] Finally, the acidic pK_a value at 2.45 was attributed to the protonation of the bipyridyl core. Although quite more acidic than that measured for simple bipyridine (log K_{BipyH} = 4.39 and log K_{BipyH2} = 1.45),[37] the assignment was confirmed by absorption spectrophotometric data, evidencing the bathochromic shift of the $\pi \rightarrow \pi^*$ transitions centered on the bipyridine unit associated with the trans to cis isomerization upon protonation (Figures S17 and S18 in the Supporting Information). This feature is in agreement with the values reported for a bipyridine substituted by two aminomethyl groups (pK_a = 1.2(2)).[16]

The pK_a values of the free ligand being accurately determined, potentiometric titrations were carried out on equimolar mixtures of L and $Ln(ClO_4)_3$ salts (Ln(III) = La(III), Eu(III), Lu(III)) in water at a fixed ionic strength (0.1 M $NaClO_4$, Figure S15 in the Supporting Information). Table 2 summarizes the stability constants obtained for the formation of the mononuclear LnL complexes and the associated measured protonation constants. Interestingly, the log K_{LnL} values are very similar along the Ln(III) series, ranging from 19.5 to 19.8 log units. For Ln(III) coordination, the general trends observed in complex stability are (i) an increase of log K with Z associated with stronger electrostatic interactions due to the lanthanidic contraction, as for EDTA,[38] (ii) a bell-shaped curve with a maximum around the middle of the series, as observed for DTPA,[39] and (iii) in a few cases, a drop of log K with increasing Z.[40] This unusual case of constant K within the Ln(III) series may be related to a subtle equilibrium between different driving forces. On the one hand, the increasing electrostatic attraction between the trivalent cation and the negatively charged ligand favors an increased complex stability for the heavier Ln. At the opposite, the more negative hydration free energies of the Ln(III) ion along the lanthanide series[41] and the larger electrostatic repulsions of the negative charges of the phosphonate functions (see DFT Modeling of the Polynuclear Species) would tend to destabilize the formation of the complex with increasing Z.

Unexpectedly, the addition of an additional pyridine had a dramatic influence on the global stability of the LnL complexes, the log K values dropping by more than 6 orders of magnitude in comparison to those with L_P.[9] It is surmised that the introduction of the second pyridine unit tends to move the phosphonated functions closer, resulting in larger electrostatic repulsions and an overall destabilization of the coordination of Ln(III) cations. Nevertheless, the thermodynamic stability is quite high and the calculated pLn values[42] are interesting and sufficient for potential biological applications. The species distribution diagram as a function of pH for the LuL complex is presented in Figure S19 in the Supporting Information and shows that, at neutral pH, the complexes are essentially present as the mono- and diprotonated species $[LuLH]^{4-}$ and $[LuLH_2]^{3-}$, respectively. In view of the important negative charges, it is not surprising that the mononuclear complexes form polynuclear species in the presence of excess of Ln cations. Absorption and emission spectrophotometric titrations conducted at acidic pH (pH 2, Figures S36−S41 in the Supporting Information) further confirm the presence of mononuclear monochelates.

Synthesis of the [LnL] Complexes (Ln = La, Tb, Yb, Lu). Considering the rather high stability of the [LnL] species, the mononuclear complexes of La(III), Tb(III), Yb(III), and Lu(III) were prepared and isolated by mixing stoichiometric amounts of the ligands and the corresponding Ln(III) salts. Elemental analysis supported the 1:1 stoichiometry of the complexes, which were isolated at neutral pH and were in agreement with the presence of four sodium counterions. The isotopic distributions and charge patterns observed by ESI mass spectrometry further substantiated the complexes to be mononuclear, with a $[LnLH]Na_4$ composition.

In view of the impossibility to get a crystal structure of one of these isolated complexes in our hands, we turned our attention to the modeling of the complexes by DFT. Figure 3 represents the models obtained for the Yb(III) complex in its fully deprotonated form. From this model, it is confirmed that the cation is fully chelated into the cavity formed by the octadentate ligand. The wrapping of the ligand resulted in an overall pseudo-C_2 symmetry, the C_2 axis passing through the Yb(III) atom and the middle of the C−C bond joining the two pyridyl groups. Considering the average plane formed by the bipyridine, the phosphonate functions are coordinated according to two different modes. Two phosphonate groups, one from each iminomethylbisphosphonate function, are almost in the plane, whereas the two remaining groups are situated on the top and on the bottom of the structure being coordinated in an out-of-plane mode. A particularly striking feature of the model is the distribution of electrostatic potential, as computed on the molecular surface defined by a 0.001 electron bohr^{-3} contour of the electronic density.[43] The region of the phosphonate coordination is highly negatively charged (Figure 3c,d), corroborating the hypothesis of a decreased coordination strength of L in comparison to L_P due to increased electrostatic repulsions of the charges in L and thus explaining the propensity of the LnL species to form polynuclear complexes with an excess of added Ln(III) cations in solution. Indeed, the DFT optimized structure obtained for $[YbL]^{5-}$ presents two O···O distances involving the coordinated oxygen atoms of the phosphonate groups as short as 2.93 and 3.10 Å, while these distances calculated for $[YbL_P]^{5-}$ are much longer (3.19 and 3.45 Å).[9]

The La(III) and Lu(III) complexes were further examined by ^1H, ^{13}C, and ^{31}P NMR spectroscopy (Figures S20−S25 in the Supporting Information) and by ^1H NMR for the Yb(III) complex (Figure S36 in the Supporting Information). While the aromatic part of the ^1H NMR spectra displays the expected pattern of two doublets and a triplet, the aliphatic regions present broad and poorly resolved signals, with the signals due to the methylene bridges joining the tertiary amines to the phosphonate functions being even too broad to be observed in the case of the La(III) complex. It is surmised that the in-plane and out-of-plane phosphonate functions are prone to an interconversion process, as observed for similar polycarboxylated[44] and polyphosphonated complexes.[9] The presence of two magnetically nonequivalent phosphonate functions is further substantiated by the observation of two signals in the ^{31}P NMR spectrum of the Lu(III) complex (Figure S23). For the neighboring paramagnetic Yb(III) atom, the ^1H NMR spectrum (Figure S36) is composed of nine peaks of equal intensity spread out over more than 40 ppm. The spectrum is in agreement with an average C_2 symmetry, with a slow exchange of the in-plane and out-of-plane functions.

In contrast, the ^{31}P NMR spectrum of the La(III) complex only displayed one peak (Figure S25 in the Supporting Information), pointing to a faster exchange on the NMR time scale for the larger La(III) cation, which can be reasonably explained by weaker electrostatic interactions leading to a faster interconversion process. The ^{13}C NMR spectra are also in agreement with this kinetic profile, the fast exchange of the La(III) complex leading to the observation of a doublet of doublets ($^1J_{PC}$ = 142 Hz, $^3J_{PC}$ = 8 Hz) for the two equivalent phosphonate methylene bridges and a triplet for the methylene bridge joining the pyridyl rings to the tertiary amine that couples with two equivalent P atoms (Figure S20 in the Supporting Information). For the Lu(III) complex (Figure S22 in the Supporting Information), the corresponding signals become a very broad peak at ca. 60 ppm and a broad singlet at 66.0 ppm, the broadening being attributed to the coalescence for these C atoms at 100 MHz.

Considering the high thermodynamic stability of the LnL complexes, we were also interested in testing their kinetic inertness in the presence of an excess of lanthanide cations in solution. A first set of experiments consisted of monitoring the evolution of the ^1H and ^{31}P NMR spectra of solutions of the isolated LaL (or LuL) complexes upon addition of increasing amounts of $LuCl_3$ (or $LaCl_3$). Considering the differences, especially in the pattern of the ^{31}P spectra, a metal exchange within the cavity from La to Lu would result in a change from a singlet (La) to a broad doublet (Lu). Addition of increasing amounts of $LuCl_3$ from 0 to 5 equiv to the solution of LaL in D_2O (pD 7.4) did not result in any significant change in either the ^1H or the ^{31}P spectra (Figures S24 and S25 in the Supporting Information, respectively). It was then decided to heat the solution to 80 °C to increase the possibly kinetically slow process, but even after 1 month at 80 °C, no evidence of exchange could be detected in the corresponding NMR spectra (Figures S24 and S25). Although this result was prone to indicate a very slow exchange, the possibility of a very fast exchange resulting in a coalescence of the LuL and LaL signals of the complex into a singlet should not be discarded at that step. In addition, the appearance of a broad doublet in the ^{31}P spectra may be hidden in the baseline for small quantities of LuL complexes formed. To discard the hypothesis of a fast exchange, the reverse experiment was similarly performed by adding increasing amounts of $LaCl_3$ salts from 0 to 5 equiv to a LuL solution in D_2O (pD 7.4, Figure S26 in the Supporting Information). Addition of 0.25 and 0.5 equiv resulted in no significant change of the spectra, but after further addition of

DOI: 10.1021/acs.inorgchem.6b02414
Inorg. Chem. XXXX, XXX, XXX−XXX

$LaCl_3$ up to 5 equiv, the signals of the methylene bridges of the aliphatic regions all broadened, with no change in the chemical shifts. Concerning the ^{31}P spectra (Figure S27 in the Supporting Information), absolutely no change could be observed and this was further confirmed even after heating the sample for 1 month at 80 °C. A direct conclusion of these sets of experiments is that the complexes are not only thermodynamically very stable but also kinetically stable at high temperature in water for 1 month at neutral pH.

In order to strengthen the characterization of the polynuclear species formed in excess of Ln(III) cations, we performed further titration experiments by addition of $TbCl_3$ to the isolated TbL mononuclear complex in water (ammonium formiate buffer, pH 7.0, 0.01 M) while monitoring the evolution with electrospray ionization (ESI) and matrix-assisted laser desorption (MALDI) mass spectra. While both the positive and negative ionization modes were studied, only the positive mode afforded signals with sufficient intensities. Nevertheless, even in the positive mode, the signals were so weak that it was necessary to further add trifluoroacetic acid to the solutions, decreasing the pH to 2.0, to afford sufficient current intensity. The ES/MS spectrum of the TbL complex (Figure 4) displays a series of peaks separated by 22 m/z units, which could be attributed to the $[TbLH_{6-x}Na_x]^+$ species with $x = 0–6$, respectively (L stands for the fully deprotonated ligand). The assignments of the peaks observed during the ESI-MS titration can be found in Table 3. Addition of 0.5 equiv of Tb(III) showed only minor variations (Figure S28 in the Supporting Information). For 1 equiv of added Tb(III), the spectrum became far more complicated with numerous peaks appearing in the m/z 900–1150 region. Among the new peaks, a family can be distinguished as originating from $[Tb_4L_2H_{6-x}Na_x]^{2+}$ species ($x = 0–4$), the doubly charged character being translated into a 0.5 m/z unit spacing between the peaks in the isotopic distributions. It is noteworthy that, for even values of x, the peaks can also correspond to $[Tb_2LH_{3-y}Na_y]^+$ ($y = 0–2$) monocharged species (i.e., $y = x/2$), pointing to the presence of dinuclear Tb complexes with a single ligand.

In fact, the dinuclear species can also be identified with monocharged peaks corresponding to $[Tb_2LH_3{\cdot}H_2O]^+$ and $[Tb_2LH_2Na{\cdot}H_2O]^+$. Whether these dinuclear species are present in solution or are the fragmentation products of the tetranuclear complexes could not be deciphered herein. Finally, the region between m/z 980 and 1015 also displayed numerous peaks that could be safely attributed to $[Tb_5L_2H_{3-x}Na_x{\cdot}yH_2O]^{2+}$ ($x = 0–3$; $y = 0–2$) species, confirming the presence of the pentanuclear Tb complex in solution as previously assessed by UV–vis absorption and luminescence spectroscopic titrations.

In the case of MALDI experiments, the same acidic treatment (addition of TFA) was also necessary. Unfortunately, the titration was not conclusive, apart from the observation of the molecular peak of the $[TbLH_6]^+$ species (observed at m/z 747.162) and for a weak peak at m/z 1649.09 units in the presence of added Tb(III) salts (Figure S29 in the Supporting Information). This species was attributed to the presence of the trinuclear Tb(III) complex $[Tb_3L_2H_8]^+$, which is expected at m/z 1648.81 (for $C_{32}H_{44}N_8O_{24}P_8Tb_3$). In conclusion, although the mass spectrometric titrations were performed under acidic conditions, they confirmed the presence of all the species already observed by spectrophotometric titrations at neutral pH.

DFT Modeling of the Polynuclear Species. To get insights into the structures of the polynuclear species, we turned again our interest toward DFT modeling. Figure 5 represents the DFT models of the $[(YbL)_2Yb_x]$ ($x = 1–3$) complexes obtained. It is noteworthy that, on the basis of the spectroscopic data previously obtained, the two first Yb(III) atoms (numbered Yb1 and Yb2) were constrained into the cavity of the two L ligands and these entities are denoted (YbL), the coordination of the incoming Yb(III) atoms being screened with DFT. In the trinuclear species, the third Yb(III) atom (Yb3) is sandwiched by the two (YbL) complexes and is coordinated by the two in-plane phosphonate functions (see the modeling of the (YbL) complex above for the definition of in-plane and out-of-plane phosphonate functions). Each (YbL) complex acts as a tridentate ligand. The coordination sphere was completed by the addition of a water molecule. One of the two in-plane phosphonate function of each (YbL) complex acts as a bridging bidentate ligand being coordinated by the oxygen atom implicated in the coordination to the Yb(III) atom of Yb1 (or Yb2) and by a second O atom. For the second in-plane phosphonate, the coordination is only occurring by an O atom not coordinated to the Yb atom of the (YbL) complexes. The overall arrangement of the three Yb(III) cations is almost linear (Yb1–Yb3–Yb2 angle of 163°), and the distances between the central and peripheral Yb(III) atoms are 4.43 and 4.45 Å, respectively, for Yb1 and Yb3.

In the tetranuclear complex, the coordination around the central Yb(III) atom is almost unchanged in comparison to the trinuclear complex, with a small lengthening of the Yb1–Yb3 and Yb3–Yb2 distances (4.51 and 4.53 Å, respectively). The fourth Yb atom is coordinated by one of the in-plane phosphonate function of the (Yb1L) complex in a bidentate mode and further linked to (Yb2L) by one of the out-of-plane phosphonate functions. The coordination of the fourth Yb(III) atom was fulfilled by three water molecules added in the model. Interestingly, the arrival of this supplementary Ln(III) cation did not significantly perturb the system and only a small bending of the Yb1–Yb3–Yb2 angle to 160° can be observed. In the system, the central Yb3 atom was found to be at almost equivalent distances from Yb1 (4.51 Å), Yb2 (4.53 Å), and Yb4 (4.40 Å).

Coordination of the fifth Yb(III) cation was predicted to occur opposite to Yb4 and was obtained by one in-plane phosphonate function of Yb1, one in-plane function of Yb2, and the second out-of-plane function of Yb2 at the opposite of Yb4. In this case as well, the coordinations of Yb4 and Yb5 were further completed by water molecules (four) implemented in the model. As for the tetranuclear compound, the introduction of this fifth Yb(III) atom did not greatly perturb the pre-existing assembly, with a slight bending of the Yb1–Yb3–Yb2 angle to 158°, together with a shortening of the Yb1–Yb3 and Yb3–Yb2 distances to 4.40 and 4.44 Å, respectively, while Yb4 and Yb5 were found to be at 4.20 and 3.81 Å from the central Yb3, respectively.

In conclusion, although great care must be taken in the use of DFT models, those tend to show that the introductions of the fourth and fifth Yb atoms did not bring much change to the structure of the trinuclear complex precursor, the incoming Yb(III) cations being adequately coordinated by the numerous pending phosphonate functions. This is in line with the very weak changes observed in the absorption spectra of the complexes upon formation of the polynuclear species, explaining the easy formation of these polynuclear species and their observation by spectrophotometric or mass spectrometric techniques.

CONCLUSION

Ligand L is an attractive ligand for the coordination of lanthanide cations, forming thermodynamically and kinetically stable mononuclear LnL complexes. Surprisingly, the introduction of an additional pyridyl unit affording a bipyridyl scaffold resulted in an important decrease of the thermodynamic stability of the complexes in comparison to those of the parent L_P ligand (containing a single pyridine in the scaffold), which are more than 6 orders of magnitude more stable. Interestingly, the addition of excess Ln(III) cations to the LnL complexes led to the formation of discrete $[(LnL)_2Ln_x]$ assemblies, which were detected by UV−vis and fluorescence spectrophotometric techniques and further confirmed by mass spectrometry. DFT modeling of the complexes suggested that the wrapping of the ligand around the Ln(III) cations led to an important charge polarization, the four phosphonate arms being gathered on one side of the complex characterized by a very negative electrostatic potential. This important local negative charge is probably at the origin of the thermodynamic destabilization of the LnL complexes in comparison to the LnL_P complexes, in which the phosphonate functions are placed at larger distances. This large local negative charge is also at the origin of the strong interactions of LnL complexes with excess Ln(III) cations if present in solution, favoring the formation of the polynuclear species. Interestingly, the kinetic inertness of the LnL complexes at neutral pH may allow the formation of controlled heteropolynuclear architectures. In the case of Ln(III) cations, such edifices would be of particular interest to control intramolecular energy transfer processes within Ln(III) cations at short distances.[46] Considering the interest of such compounds for applications to downshifting[47] or upconversion,[48] current efforts are now being devoted to a deeper understanding of the formation of controlled heteropolynuclear species.

ASSOCIATED CONTENT

Supporting Information

The Supporting Information is available free of charge on the ACS Publications website at DOI: 10.1021/acs.inorgchem.6b02414.

> UV−vis and luminescence titration of L by $TbCl_3$, full details of the fitting of the titrations of L by Tb(III) and Yb(III), potentiometric and spectrophotometric titrations of L and Ln:L (1:1, Ln = La, Eu, Lu) mixtures as a function of pH, ^1H, ^{13}C, and ^{31}P NMR spectra of **3**, L, [LaL] and [LuL] in D_2O, and [LaL] (or ([LuL]) in the presence of 0−5 equiv of $LuCl_3$ (respectively $LaCl_3$) at room temperature and after heating, and mass spectra of [TbL] in the presence of excess $TbCl_3$ (PDF)

AUTHOR INFORMATION

Corresponding Author

*E-mail for L.J.C.: l.charbonn@unistra.fr.

ORCID

Loïc J. Charbonnière: 0000-0003-0328-9842

Notes

The authors declare no competing financial interest.

ACKNOWLEDGMENTS

N.S. gratefully acknowledges the Algerian Ministry of research for financial support. C.P.-I. thanks the Centro de Supercomputación of Galicia (CESGA) for providing the computer facilities. Dr. Anne Boos and Mrs. Pascale Ronot are gratefully acknowledged for recording HPIC experiments.

REFERENCES

(1) Lukes, I.; Kotek, J.; Vojtisek, P.; Hermann, P. Complexes of tetraazacycles bearing methylphosphinic/phosphonic acid pendant arms with copper(II), zinc(II) and lanthanides(III). A comparison with their acetic acid analogues. *Coord. Chem. Rev.* **2001**, *216−217*, 287.

(2) Popov, K.; Ronkkomaki, H.; Lajunen, L. H. J. Critical evaluation of stability constants of phosphonic acids. *Pure Appl. Chem.* **2001**, *73*, 1641.

(3) Aime, S.; Botta, M.; Geninatti Crich, S.; Giovenzana, G.; Pagliarin, R.; Sisti, M.; Terreno, E. NMR relaxometric studies of Gd(III) complexes with heptadentate macrocyclic ligands. *Magn. Reson. Chem.* **1998**, *36*, S200.

(4) (a) Eliseeva, S.; Bünzli, J.-C. G. Lanthanide luminescence for functional materials and bio-sciences. *Chem. Soc. Rev.* **2010**, *39*, 189−227. (b) Sy, M.; Nonat, A.; Hildebrandt, N.; Charbonnière, L. J. Lanthanide-based luminescence biolabelling. *Chem. Commun.* **2016**, *52*, 5080.

(5) (a) Beeby, A.; Clarkson, I. M.; Dickins, R. S.; Faulkner, S.; Parker, D.; Royle, L.; de Sousa, A. S.; Williams, J. A. G.; Woods, M. Non-radiative deactivation of the excited states of europium, terbium and ytterbium complexes by proximate energy-matched OH, NH and CH oscillators: an improved luminescence method for establishing solution hydration states. *J. Chem. Soc., Perkin Trans. 2* **1999**, 493. (b) Horrocks, W. J.; Sudnick, D. R. Lanthanide Ion Luminescence Probes of the Structure of Biological Macromolecules. *Acc. Chem. Res.* **1981**, *14*, 384. (c) Doffek, C.; Seitz, M. The RadiativeLifetime in Near-IR-Luminescent Ytterbium Cryptates: The Key to Extremely High Quantum Yields. *Angew. Chem., Int. Ed.* **2015**, *54*, 9719.

(6) Balogh, E.; Mato-Iglesias, M.; Platas-Iglesias, C.; Toth, E.; Djanashvili, K.; Peters, J. A.; de Blas, A.; Rodriguez-Blas, T. Pyridine- and Phosphonate-Containing Ligands for Stable Ln Complexation. Extremely Fast Water Exchange on the Gd^{III} Chelates. *Inorg. Chem.* **2006**, *45*, 8719.

(7) Avecilla, F.; Peters, J. A.; Geraldes, C. F. G. C. X-ray Crystal Structure of a Sodium Salt of $[Gd(DOTP)]^{5-}$: Implications for Its Second-Sphere Relaxivity and the ^{23}Na NMR Hyperfine Shift Effects of $[Tm(DOTP)]^{5-}$. *Eur. J. Inorg. Chem.* **2003**, *2003*, 4179.

(8) (a) Boros, E.; Karimi, S.; Kenton, N.; Helm, L.; Caravan, P. Gd(DOTAlaP): exploring the boundaries of fast water exchange in gadolinium-based magnetic resonance imaging contrast agents. *Inorg. Chem.* **2014**, *53*, 6985. (b) Botta, M. Second Coordination Sphere Water Molecules and Relaxivity of Gadolinium(III) Complexes: Implications for MRI Contrast Agents. *Eur. J. Inorg. Chem.* **2000**, *2000*, 399.

(9) (a) Abada, S.; Lecointre, A.; Elhabiri, M.; Esteban-Gomez, D.; Platas-Iglesias, C.; Tallec, G.; Mazzanti, M.; Charbonnière, L. J. Highly relaxing gadolinium based MRI contrast agents responsive to Mg^{2+} sensing. *Chem. Commun.* **2012**, *48*, 4085. (b) Elhabiri, M.; Abada, S.; Esteban-Gomez, D.; Cassino, C.; Platas-Iglesias, C.; Botta, M.; Charbonnière, L. J. Importance of outer-sphere and aggregation phenomena in the relaxation properties of phosphonated gadolinium complexes with potential applications as MRI contrast agents. *Chem. - Eur. J.* **2015**, *21*, 6535.

(10) Brandel, J.; Lecointre, A.; Kollek, J.; Michel, S.; Hubscher-Bruder, V.; Déchamps-Olivier, I.; Platas-Iglesias, C.; Charbonnière, L. J. Tetraphosphonated thiophene ligand: mixing the soft and the hard. *Dalton Trans.* **2014**, *43*, 9070.

(11) Mukkala, V.-M.; Kwiatkowski, M.; Kankar, J.; Takalo, H. Influence of chelating groups on the luminescence properties of

Europium(III) and Terbium(III) chelates in the 2,2′-bipyridine series. *Helv. Chim. Acta* **1993**, *76*, 893.

(12) Gottlieb, H. E.; Kottyar, K.; Nudelman, A. NMR chemical shifts of common laboratory solvents as trace impurities. *J. Org. Chem.* **1997**, *62*, 7512.

(13) Bozoklu, G.; Marchal, C.; Gateau, C.; Pécaut, J.; Imbert, D.; Mazzanti, M. Diastereoselective self-Assembly of a homochiral europium triangle from a bipyoxazoline-carboxylate ligand. *Chem. - Eur. J.* **2010**, *16*, 6159.

(14) Aime, S.; Botta, M.; Garino, E.; Geninatti Crich, S.; Giovenzana, G.; Pagliarin, R.; Palmisano, G.; Sisti, M. Non-covalent conjugates between cationic polyamino acids and Gd^{III} chelates: A route for seeking accumulation of MRI-contrast agents at tumor targeting sites. *Chem. - Eur. J.* **2000**, *6*, 2609.

(15) (a) Newkome, G. R.; Puckett, W. E.; Kiefer, G. E.; Gupta, V. K.; Xia, Y.; Coreil, M.; Hackney, M. A. *α*-Methyl functionalization of electron-poor heterocycles. Chloromethyl derivatives of 2,2′-bipyridines. *J. Org. Chem.* **1982**, *47*, 4116. (b) Li, W.; Xie, J.-H.; Yuan, M.-L.; Zhou, Q.-L. Ruthenium complexes of tetradentate bipyridine ligands: highly efficient catalysts for the hydrogenation of carboxylic esters and lactones. *Green Chem.* **2014**, *16*, 4081.

(16) Wang, Z.; Reibenspies, J.; Motekaitis, R.; Martell, A. E. Unusual stabilities of 6,6′-bis(aminomethyl)-2,2′-bipyridyl chelates of transition-metal ions and crystal structures of the ligand and its copper(II) and nickel(II) complexes. *J. Chem. Soc., Dalton Trans.* **1995**, 1511.

(17) Tao, J.; Perdew, J. P.; Staroverov, V. N.; Scuseria, G. E. Climbing the density functional ladder: nonempirical meta−generalized gradient approximation designed for molecules and solids. *Phys. Rev. Lett.* **2003**, *91*, 146401.

(18) Frisch, M. J.; Trucks, G. W.; Schlegel, H. B.; Scuseria, G. E.; Robb, M. A.; Cheeseman, J. R.; Scalmani, G.; Barone, V.; Mennucci, B.; Petersson, G. A.; Nakatsuji, H.; Caricato, M.; Li, X.; Hratchian, H. P.; Izmaylov, A. F.; Bloino, J.; Zheng, G.; Sonnenberg, J. L.; Hada, M.; Ehara, M.; Toyota, K.; Fukuda, R.; Hasegawa, J.; Ishida, M.; Nakajima, T.; Honda, Y.; Kitao, O.; Nakai, H.; Vreven, T.; Montgomery, J. A., Jr.; Peralta, J. E.; Ogliaro, F.; Bearpark, M.; Heyd, J. J.; Brothers, E.; Kudin, K. N.; Staroverov, V. N.; Kobayashi, R.; Normand, J.; Raghavachari, K.; Rendell, A.; Burant, J. C.; Iyengar, S. S.; Tomasi, J.; Cossi, M.; Rega, N.; Millam, J. M.; Klene, M.; Knox, J. E.; Cross, J. B.; Bakken, V.; Adamo, C.; Jaramillo, J.; Gomperts, R.; Stratmann, R. E.; Yazyev, O.; Austin, A. J.; Cammi, R.; Pomelli, C.; Ochterski, J. W.; Martin, R. L.; Morokuma, K.; Zakrzewski, V. G.; Voth, G. A.; Salvador, P.; Dannenberg, J. J.; Dapprich, S.; Daniels, A. D.; Farkas, Ö.; Foresman, J. B.; Ortiz, J. V.; Cioslowski, J.; Fox, D. J. *Gaussian 09 Revision D.01*; Gaussian, Inc., Wallingford, CT, 2009.

(19) Dolg, M.; Stoll, H.; Savin, A.; Preuss, H. Energy-adjusted pseudopotentials for the rare earth elements. *Theor. Chim. Acta* **1989**, *75*, 173.

(20) Tomasi, J.; Mennucci, B.; Cammi, R. Quantum mechanical continuum solvation models. *Chem. Rev.* **2005**, *105*, 2999.

(21) Rappe, A. K.; Casewit, C. J.; Colwell, K. S.; Goddard, W. A.; Skiff, W. M. UFF, a full periodic table force field for Molecular mechanics and molecular dynamics simulations. *J. Am. Chem. Soc.* **1992**, *114*, 10024.

(22) Méthodes d'Analyses Complexométriques avec les Titriplex, Ed. Merck, Darmstadt, Germany.

(23) Raymond, K. N. Chemical safety. *Chem. Eng. News* **1983**, *61*, 4.

(24) Gans, P.; O'Sullivan, B. GLEE, a new computer program for glass electrode calibration. *Talanta* **2000**, *51*, 33.

(25) (a) Gans, P.; Sabatini, A.; Vacca, A. A. *HYPERQUAD 2000*; Leeds, U.K., and Florence, Italy, 2000. (b) Gans, P.; Sabatini, A.; Vacca, A. A. Investigation of equilibria in solution. Determination of equilibrium constants with the HYPERQUAD suite of programs. *Talanta* **1996**, *43*, 1739.

(26) Gans, P. *Data Fitting in the Chemical Sciences*; Wiley: Chichester, U.K., 1992.

(27) Gampp, H.; Maeder, M.; Meyer, C. J.; Zuberbühler, A. D. Calculation of equilibrium constants from multiwavelength spectroscopic data—I: Mathematical considerations. *Talanta* **1985**, *32*, 95.

(28) Gampp, H.; Maeder, M.; Meyer, C. J.; Zuberbühler, A. D. Calculation of equilibrium constants from multiwavelength spectroscopic data—II132, 95.: Specfit: two user-friendly programs in basic and standard fortran 77. *Talanta* **1985**, *32*, 257.

(29) Gampp, H.; Maeder, M.; Meyer, C. J.; Zuberbühler, A. D. Calculation of equilibrium constants from multiwavelength spectroscopic data—III: Model-free analysis of spectrophotometric and ESR titrations. *Talanta* **1985**, *32*, 1133.

(30) Marquardt, D. W. An algorithm for least-squares estimation of nonlinear parameters. *J. Soc. Ind. Appl. Math.* **1963**, *11*, 431.

(31) Maeder, M.; Zuberbühler, A. D. Nonlinear least-squares fitting of multivariate absorption data. *Anal. Chem.* **1990**, *62*, 2220.

(32) Nakamoto, K. Ultraviolet spectra and structures of 2,2′-bipyridine and 2,2′,2″-terpyridine in aqueous solution. *J. Phys. Chem.* **1960**, *64*, 1420.

(33) (a) Prodi, L.; Montalti, M.; Zaccheroni, N.; Pickaert, G.; Charbonnière, L.; Ziessel, R. New europium(III) complexes containing hybrid ligands with hard and soft complexation centres. *New J. Chem.* **2003**, *27*, 134. (b) Charbonnière, L. J.; Weibel, N.; Retailleau, P.; Ziessel, R. Relationship between the ligand structure and the luminescent properties of water-soluble lanthanide complexes containing bis(bipyridine) anionic arms. *Chem. - Eur. J.* **2007**, *13*, 346.

(34) Comby, S.; Bünzli, J.-C. G. Lanthanide near-infrared luminescence in molecular probes and devices. In *Handbook on the Physics and Chemistry of Rare Earths*; Gschneidner, K. A., Jr., Bünzli, J.-C. G., Pecharsky, V. K., Eds.; Elsevier: Amsterdam, 2007; Vol. *37*, p 217.

(35) (a) D'Aléo, A.; Bourdolle, A.; Brustlein, S.; Fauquier, T.; Grichine, A.; Duperray, A.; Baldeck, P. L.; Andraud, C.; Brasselet, S.; Maury, O. Ytterbium-based bioprobes for near-infrared two-photon scanning laser microscopy imaging. *Angew. Chem., Int. Ed.* **2012**, *51*, 6622. (b) Alpha, B.; Ballardini, R.; Balzani, V.; Lehn, J.-M.; Perathoner, S.; Sabbatini, N. Antenna effect in luminescent lanthanide cryptates: A photophysical study. *Photochem. Photobiol.* **1990**, *52*, 299.

(36) (a) Popov, K.; Ronkkomaki, H.; Lajunen, L. H. J. Critical evaluation of stability constants of phosphonic acids. *Pure Appl. Chem.* **2001**, 73, 1641. (b) Ichikawa, T.; Sawada, K. Protonation behavior and intramolecular interactions of *α*,*ω*-alkanediaminepolymethylenepolyphosphonates. *Bull. Chem. Soc. Jpn.* **1997**, *70*, 829. (c) Ichikawa, T.; Sawada, K. Structure and NMR Behavior of Cobalt(III) Polyamine Complexes of *α*,*ω*-Alkylenediamine-N,N,N′,N′-tetramethylenetetraphosphonate in Aqueous Solution. *Bull. Chem. Soc. Jpn.* **1997**, *70*, 2111.

(37) Abbas Abbasi, S.; Bhat, B.; Singh, R. Mixed ligand complexes involving hydroxamic acids I. Complexes of benzohydroxamic acid in aqueous solutions. *Inorg. Nucl. Chem. Lett.* **1976**, *12*, 391.

(38) (a) Caravan, P.; Hedlund, T.; Liu, S.; Sjöberg, S.; Orvig, C. Potentiometric, calorimetric, and solution NMR studies of a tridentate ligand which has a marked preference for formation of bis(1igand) versus mono(1igand) lanthanide complexes and which exhibits high selectivity for heavier lanthanides. *J. Am. Chem. Soc.* **1995**, *117*, 11230. (b) Chapon, D.; Morel, J.-P.; Delangle, P.; Gateau, C.; Pécaut, J. Lanthanide(III) complexation by the ligand 1,3,5-triamino-1,3,5-trideoxy-*cis*-inositol: an unusual thermodynamic behaviour across the rare-earth series. *Dalton Trans* **2003**, 2745.

(39) Sarka, L.; Banyai, I.; Brücher, E.; Kiraly, R.; Platzek, J.; Radüchel, B.; Scmitt-Willich, H. J. Synthesis, equilibrium and NMR studies of lanthanide(III) complexes of the N-mono(methylamide) and N′-mono(methylamide) derivatives of diethylenetriamine-N,N,N′,N″,N″-pentaacetic acid. *Chem. Soc. Dalton Trans.* **2000**, 3699.

(40) (a) Chang, C. A.; Rowland, M. E. Metal complex formation with 1,10-diaza-4,7, 13,16-tetraoxacyclooctadecane-N,N′-diacetic acid. An approach to potential lanthanide ion selective reagents. *Inorg. Chem.* **1983**, *22*, 3866. (b) Roca-Sabio, A.; Mato-Iglesias, M.; Esteban-Gómez, D.; Toth, E.; de Blas, A.; Platas-Iglesias, C.; Rodriguez-Blas, T. Macrocyclic receptor exhibiting unprecedented selectivity for light lanthanides. *J. Am. Chem. Soc.* **2009**, *131*, 3331.

DOI: 10.1021/acs.inorgchem.6b02414
Inorg. Chem. XXXX, XXX, XXX−XXX

(41) Regueiro-Figueroa, M.; Esteban-Gómez, D.; de Blas, A.; Rodríguez-Blas, T.; Platas-Iglesias, C. Understanding stability trends along the lanthanide series. *Chem. - Eur. J.* **2014**, *20*, 3974.

(42) Harris, W. R.; Carrano, C. J.; Raymond, K. N. Spectrophotometric determination of the proton-dependent stability constant of ferric enterobactin. *J. Am. Chem. Soc.* **1979**, *101*, 2213.

(43) Bader, R. F. W.; Carroll, M. T.; Cheeseman, J. R.; Chang, C. Properties of atoms in molecules: atomic volumes. *J. Am. Chem. Soc.* **1987**, *109*, 7968.

(44) Mato-Iglesias, M.; Rodriguez-Blas, T.; Platas-Iglesias, C.; Starck, M.; Kadjane, P.; Ziessel, R.; Charbonnière, L. J. Solution structure and dynamics, stability, and NIR emission properties of lanthanide complexes with a carboxylated bispyrazolylpyridyl ligand. *Inorg. Chem.* **2009**, *48*, 1507.

(45) Patiny, L.; Borel, A. ChemCalc: A Building Block for Tomorrow's Chemical Infrastructure. *J. Chem. Inf. Model.* **2013**, *53*, 1223.

(46) Nonat, A.; Figueiro-Rigueroa, M.; Esteban-Gómez, D.; de Blas, A.; Rodríguez-Blas, T.; Platas-Iglesias, C.; Charbonnière, L. J. Definition of an intramolecular Eu-to-Eu energy transfer within a discrete [Eu_2L] complex in solution. *Chem. - Eur. J.* **2012**, *18*, 8163.

(47) (a) Hovel, H. J.; Hodgson, R. T.; Woodall, J. M. The effect of fluorescent wavelength shifting on solar cell spectral response. *Sol. Energy Mater.* **1979**, *2*, 19. (b) Fix, T.; Nonat, A.; Imbert, D.; Di Pietro, S.; Mazzanti, M.; Slaoui, A.; Charbonnière, L. J. Enhancement of silicon solar cells by downshifting with Eu and Tb coordination complexes. *Prog. Photovoltaics* **2016**, *24*, 1251.

(48) (a) Chen, G.; Qiu, H.; Prasad, P. N.; Chen, X. Upconversion nanoparticles: design, nanochemistry, and applications in theranostics. *Chem. Rev.* **2014**, *114*, 5161. (b) Nonat, A.; Chan, C. F.; Liu, T.; Platas-Iglesias, C.; Liu, Z.; Wong, W.-T.; Wong, W.-K.; Wong, K.-L.; Charbonnière, L. J. Room temperature molecular up conversion in solution. *Nat. Commun.* **2016**, *7*, 11978.